UDC 539.4

Numerical Simulation of Flexible Riser under Torsion

M. S. Liu,[a] X. W. Liu,[b] J. Y. Li,[a] and J. S. Ju[a,1]

[a] College of Water Resources and Civil Engineering, China Agricultural University, Beijing, China

[b] Huadian Heavy Industries Co., Ltd., Beijing, China

[1] jujinsan@cau.edu.cn

The 10-layer unbonded flexible riser is modeled with parametric modeling technology in FEM and the model is imported into ABAQUS to simulate the riser's mechanical behavior under the load condition: torsion. FEM model considering material nonlinearity and nonlinear boundary conditions (the interaction between layers) has been set to simulate the structure of riser exactly. Based on the detailed finite element model, the influence of friction coefficient on the calculation results of the riser under torsion force is studied. The computation demonstrates that there is great difference between layers and the tension armor (consisted of steel strips) is the main bearing layer. Besides, the friction coefficient has great influence on the result of the calculation.

Keywords: unbonded flexible riser, ten separate cylindrical layers, ABAQUS, frictional coefficient.

Introduction. The flexible riser studied in this paper is an assembled pipe composed of several layers and is widely used in the modern offshore structures and oil industry. The connections between layers are ensured through the structural measures rather than adhesive agent. The complex make-up of flexible riser leads to smaller radii of curvature with the same pressure capacity than rigid steel riser. Under the increasing application of ultra-deep-water structure in modern architecture, the researches of unbonded flexible riser are urgently needed.

Most researchers studied the mechanical behavior of the unbonded flexible riser through two kinds of research methods: analytical methods and finite-element models. Several analytical works have been conducted on the analytical formulations of the unbounded flexible riser under different load conditions. As one of the first scholars to study the mechanical behavior of the flexible riser, in Knapp's [1] study, the stiffness matrix cable is derived subjected to tension and torsion for a helically armored assuming that the displacements and strains of the layers are small and neglect the strength and stiffness except for the steel layers. In analytical study, there are many simplifying assumptions due to the complexity of the theoretical derivation, which significantly reduces the credibility of the calculation results. Almost all the analytical formulations studied ignore the contact and/or frictional effects [2–7]. Lanteigne [6] and McNamara and Harte [7] addressed the behavior of the helically armored cables under general set of loads and pressure and their models are capable of estimating slip, wear, collapse, tendon failure and rupture of the carcass.

The analytical models of flexible riser are quite complicated and the application range of the analytical formulations is limited by the simplified assumptions on which they are based. Almost all the weakness in analytical methods can be overcome using finite-element analyses. The layers of the flexible riser can be set up respectively with the numerical modeling method. Particularly, the interaction between layers can be considered in FEM and all loads (tension, bending moment and shear) in each layer can be fully captures. Under different stress conditions, the interaction between layers led to the complex stress distribution. The disadvantages of the FEM method are the tedious modeling processes and long computing time.

The mechanical behavior of the riser is derived from the complex make-up of the layers, so several works [8–10] have been conducted on this subject. The most FEM researches [8–10] on the flexible riser took the following pathway: the layers are modeled separately and assembled together with contact elements, and then the stress analyses are conducted under various load conditions.

The numerical simulation draws the more accurate result of stress analysis than analytical works. However, the complex modeling process and the application scope limitation of the results caused by the single model size hindered the development of FEM. In this paper, the general contact interaction with friction between all surfaces of the whole structure is set as the research variable to verify the accuracy of the assumption that ignores the contact and/or frictional effects and with this study, the calculation error caused by this assumption can be given.

1. **Finite Element Model and Material Properties**. The finite-element model of the flexible riser is developed in a global cylindrical coordinate system. The system' origin located at bottom end center of the riser. The 2m model which consists of ten separate cylindrical layers is shown as Fig. 1. Ten separate cylindrical layers are modeled by parametric modeling procedure due to the layers model with certain regularity and the complication of the structure. The 2m finite element model consists of ten layers is shown as Fig. 1. The detailed dimensions of the riser's cross section composed of 10-layer element model are shown as Fig. 2.

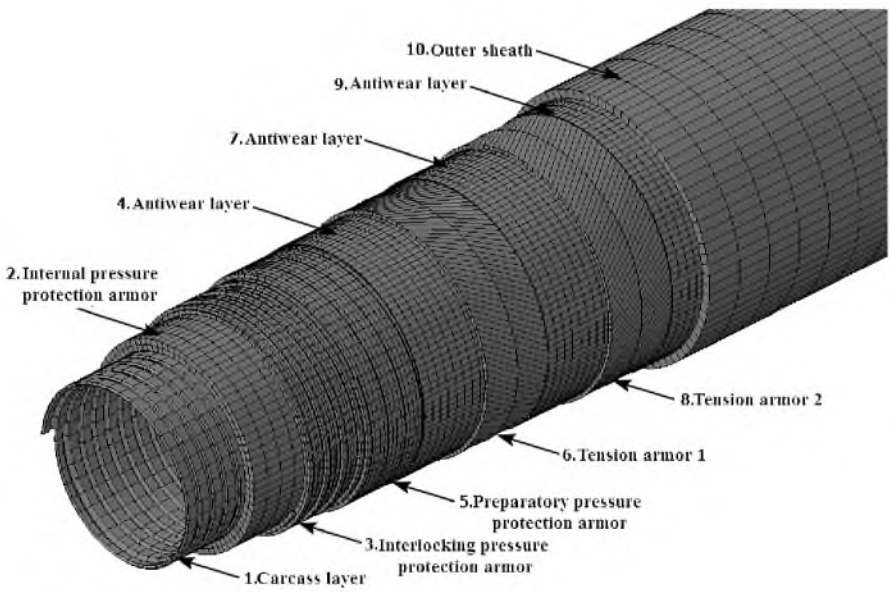

Fig. 1. Ten layers' riser.

Table 1 shows the sequence of layers and the material properties for each layer from inside to outside (the number of layers corresponds to the number shown in Fig. 1). Three types of materials are adopted by the layers in the flexible riser. In the flexible riser, the carcass layer, pressure protection armor and the tension armors are assembled by steel strips. The material of the internal pressure protection armor, the antiwear layers and the outer sheath are set in lower strength than steel.

The relevant information about the elements of the layers is listed in Table 2 (from inside layer to outside layer shown as Fig. 1). The S4R in element type refers to 3D 4-node reduced-integration shell element and 3D 8-node linear brick (reduced integration element is simplified into C3D8R for short).

Table 1

Layers of the Riser and Material Property

Layer	Material	Density (kg/m^3)	Young modulus (GPa)	Poisson's ratio
1	Steel strip	7800	207	0.30
2	Low-density polyethylene	920	0.18	0.38
3	Steel strip	7800	207	0.30
4	Steel strip	7800	207	0.30
5	Nylon braid	920	0.18	0.38
6	Steel strip	7800	207	0.30
7	Nylon braid	920	0.18	0.38
8	Steel strip	7800	207	0.30
9	Nylon braid	920	0.18	0.38
10	Low-density polyethylene	920	0.18	0.38

Table 2

Relevant Information about the Elements

Layer	Element type	Number of the elements	Number of the nodes
1	S4R	55,440	61,610
2	C3D8R	25,200	38,052
3	C3D8R	113,280	2643,484
4	C3D8R	113,280	2643,484
5	C3D8R	89,000	178,712
6	C3D8R	7,772	23,664
7	C3D8R	89,000	178,712
8	C3D8R	8,040	24,480
9	C3D8R	89,000	178,712
10	C3D8R	304,092	886,177

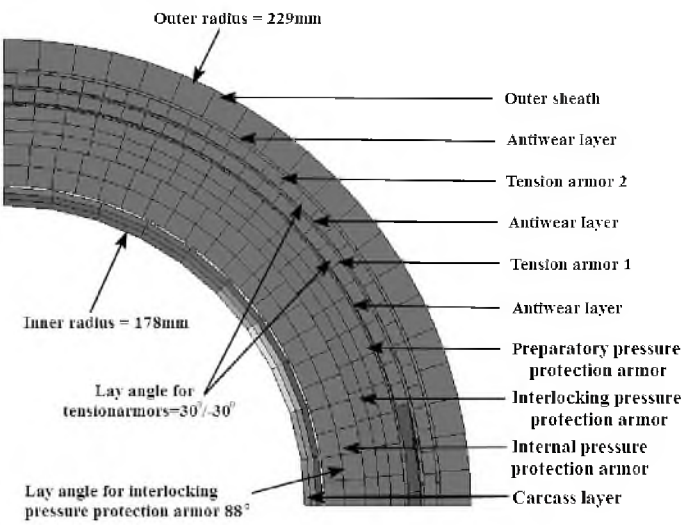

Fig. 2. Detailed geometry of riser (a quarter of the cross-sectional view).

The carcass layer is assembled together with the elements in S-shape which is close to the interlocking structure (as shown in Fig. 3). As shown in Fig. 4, the helical channel steel strips compose the interlocking pressure protection armor and preparatory pressure protection armor and combine the two layers together.

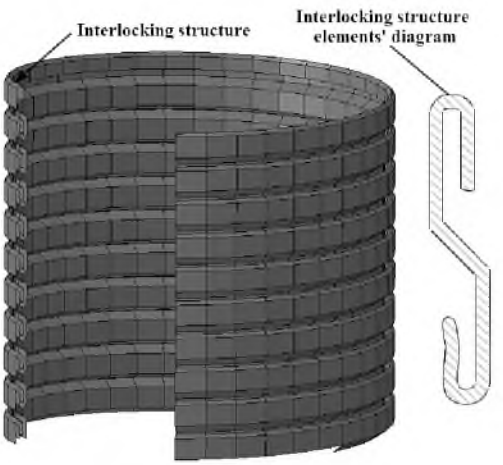

Fig. 3. Section and model of carcass layer.

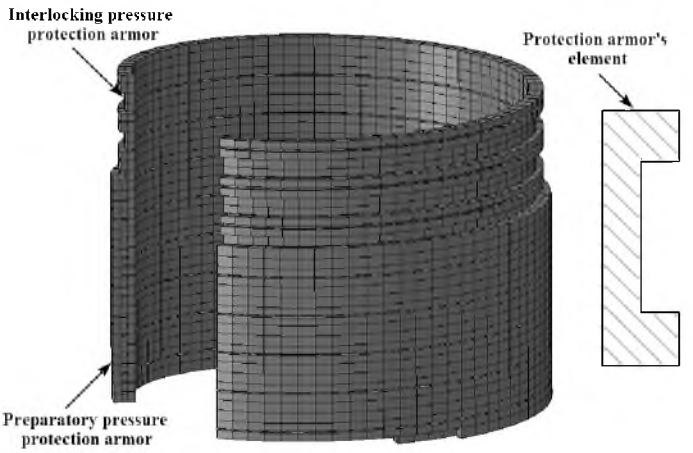

Fig. 4. Section and model of the pressure protection armor layers.

The model of the two tension layers are shown as Fig. 5. The two tension layers are composed of helical steel bars lay in opposite directions and this makes the model is unsymmetrical. So in this study, the model can't be simplified into 1/4 or 1/2 model.

The Figs. 6–8 shows the FEM model of internal pressure protection armor layer, antiwear layers and outer sheath, respectively. The antiwear layers are the protective layers modeled between preparatory pressure protection armor, tension armor 1, tension armor 2, and outer sheath.

2. **Load Case**. The FE model of riser is analyzed under torsion force with ABAQUS. The boundary conditions and load are applied to two reference points to which the ends of each side of all layers connected. In this study, the bottom end of the riser is completely constrained in all directions and rotations by constraining the reference point and the top end of the riser is totally free because the reference point connected to the top end is no constraint.

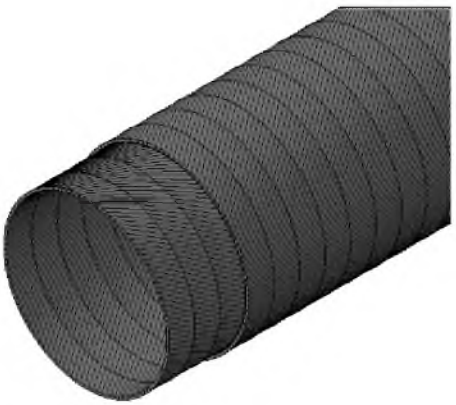

Fig. 5. Model of tension armor layers.

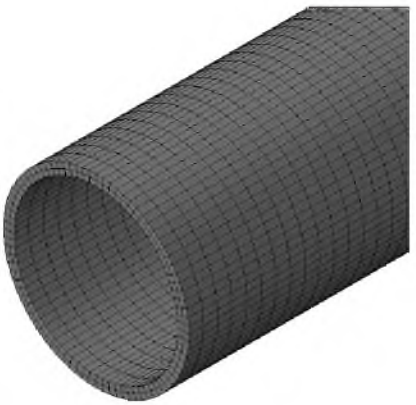

Fig. 6. Model of internal pressure protection armor layer.

Fig. 7. Model of antiwear layer.

Fig. 8. Model of outer sheath.

The finite element method in researching the riser in this study can model the layers separately. Besides, general contact interaction with friction can be defined between all surfaces of the whole structure. This includes interaction between tendons of the same tension armor layer. Because the complicated contact conditions increase the difficulty of computational convergence, the explicit solver in ABAQUS is used to carry out analysis in this study. Explicit solver without iterative calculation reduces the computing time and the sophistication requirements of the mesh.

The finite element analysis in this study is a nonlinear analysis includes both material nonlinearity in the element formulation and nonlinear boundary conditions because of the frictional contact. The highly-degree simulation of riser makes the finite-element result is more accurate than analytical result. In order to study the error resulting from ignoring the frictional effects, two examples in different contact condition are taken to analyze. In example 1, the friction coefficient is 0.1 and no friction is set in example 2.

A torsion force of 10 kN · m was applied on the reference point connected with the top end linearly with time.

3. **Calculation Results**. The maximum Mises-stress results of each layer of riser are listed in Table 3.

As shown in Table 3, Mises stress in the tension armor 1 layer is significantly larger and is greater than it in tension armor 2 as shown in Table 1. The magnitude displacement of the tension armor 1 of the two examples is shown in Fig. 9 and the magnitude displacement of the tension armor 1 is shown in Fig. 10. The deformation scale factor of

Figs. 9 and 10 is set to 3 to make the deformation more obvious. As Figs. 9 and 10 show, the steel strips in tension armor 1 are tightened and it in the tension armor 2 are relaxed which led to the difference of the internal force between tension armor 1 and tension armor 2. The graph a and graph b in Fig. 9 show the magnitude displacement of the tension armor 1 in friction coefficient $= 0.1$ and in no friction, respectively. Similarly, the graph a in Fig. 10 shows the magnitude displacement of the tension armor 1 when the friction coefficient is 0.1 and graph b in Fig. 10 shows it of the tension armor 2 in no friction.

T a b l e 3

Maximum Mises Stress of Each Layer

Contact type	Mises stress (MPa)				
	Carcass layer	Internal pressure protection armor	Interlocking pressure protection armor	Preparatory pressure protection armor	Antiwear layer
Friction =0.1	160.2	1.7	50.6	58.3	2.5
No friction	241.0	1.9	47.5	60.5	4.1
Relative error (%)	50.44	13.90	6.11	3.74	65.49
	Tension armor 1	Antiwear layer	Tension armor 2	Antiwear layer	Outer sheath
Friction =0.1	152.50	2.1	78.1	4.40	4.00
No friction	351.60	4.4	69.3	5.20	4.90
Relative error (%)	130.56	109.99	11.21	16.37	21.44

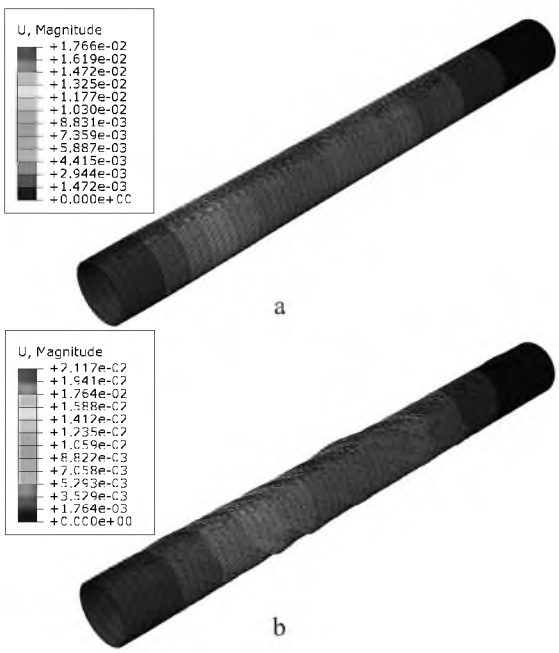

Fig. 9. The magnitude displacement of the tension armor 1 layers in different contact conditions. Here and in Figs. 10–12: (a) friction =0.1; (b) no friction. (The units of the displacement are in meters.)

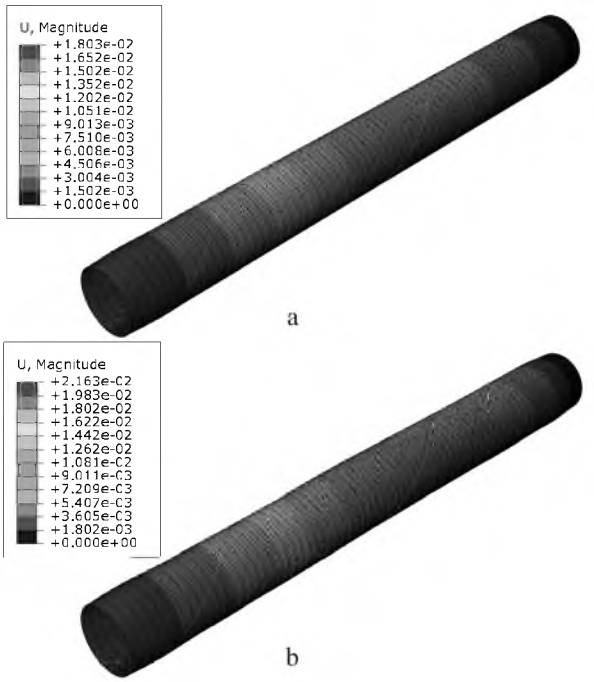

Fig. 10. The magnitude displacement of the tension armor 2 layers in different contact conditions. (The units of the displacement are in meters.)

Besides the tension armor layers, the stress distributed in the carcass layer is relatively great. So the carcass layer is the one of the main bearing layer in the riser under torsional load.

The FE model established in this research is based on torsional loading taking longitudinal, twist and radial displacement effects and besides, the contact effect is take into account. In this article, the response of the riser under torsion when the friction coefficient is set to 0.1 is assumed to be true. There is an error absolutely in the FEM analysis results without considering the friction contact effect. The maximum Mises-stress when friction coefficient $= 0.1$ shown in Table 3 is determined as the true stress and the relative error formula of the maximum Mises-stress in no friction is as follow:

$$\delta_1 = \frac{|S_1 - S_2|}{S_1},$$

where S_1 is the maximum Mises stress of each layer when friction coefficient $= 0.1$ and S_2 is the maximum Mises stress of each layer in no friction. From the relative error shown in Table 3, when there is no friction set in the model, the stress distribution of the main bearing layers (carcass layer and tension armor layers) in the riser contact has large error with the true stress distribution. The relative error of the maximum Mises stress in the tension armor 1 is the largest whose value is 130.56%.

The maximum rotation results about the longitudinal of each layer are listed in Table 4. The maximum rotation when friction coefficient $= 0.1$ shown in Table 4 is determined as the true deformation and the relative error formula of the maximum rotation in no friction is as follow:

$$\delta_2 = \frac{|U_1 - U_2|}{U_1},$$

T a b l e 4

Maximum Rotation of Each Layer

Contact type	Rotation (deg)				
	Carcass layer	Internal pressure protection armor	Interlocking pressure protection armor	Preparatory pressure protection armor	Antiwear layer
Friction =0.1	0.56597	0.63516	0.67930	0.70338	0.70968
No friction	0.69650	0.78076	0.83522	0.86446	0.87994
Relative error (%)	23.06	22.92	22.95	22.90	23.99
	Tension armor 1	Antiwear layer	Tension armor 2	Antiwear layer	Outer sheath
Friction =0.1	0.73204	0.73777	0.76070	0.76643	0.81860
No friction	0.89885	0.90631	0.93382	0.94070	1.00490
Relative error (%)	22.79	22.84	22.76	22.74	22.76

where U_1 is the maximum rotation of each layer in riser when friction coefficient $= 0.1$ and U_2 is the maximum rotation of each layer in no friction.

It can be concluded with observing Table 4 that the difference of the maximum rotation between the each layers are rather small and the relative error value of the maximum rotation in no friction of the different layers are basically the same.

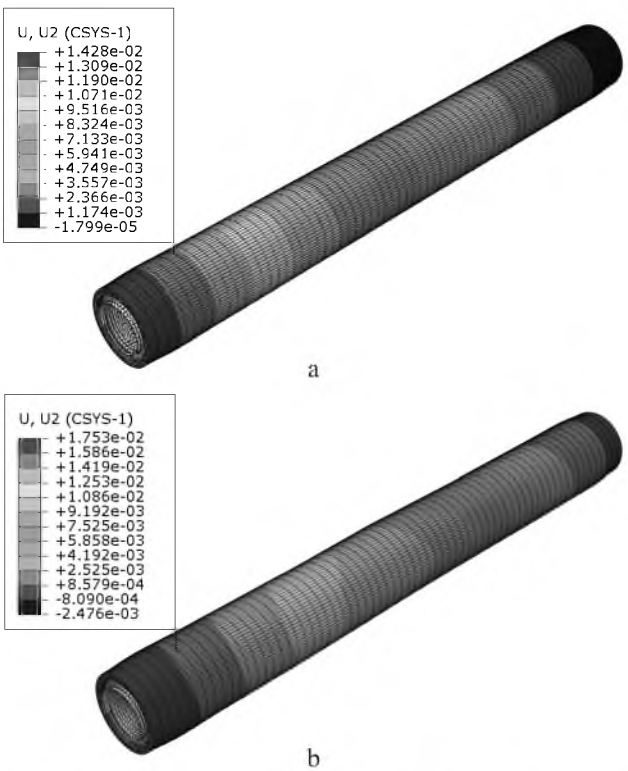

Fig. 11. The rotation of the riser about its longitudinal axis. (The units of the rotation are in radians.)

Figure 11 shows the rotation of the riser about its longitudinal axis. From the cloud diagram of the riser, it can be observed that the rotational deformation of the riser when the friction is 0.1 is basically same around the same circle and the angle of rotation is dependent of the z-coordination. But the rotational deformation of the riser is not uniform around the same circle when there is no friction defined.

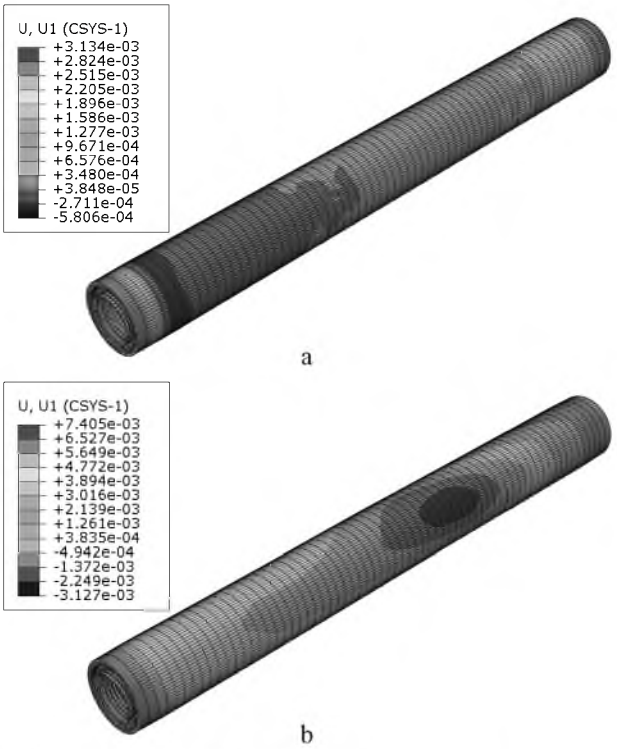

Fig. 12. Radial deformation of the riser. (The units of the displacement are in meters.)

The radial deformation of the riser is shown in Fig. 12. From the cloud diagram of the riser, it can be observed that the radial deformation of the riser when the friction coefficient = 0.1 is more uniform than it of the riser in no friction contact set. The value of the radial deformation of the riser when no friction is set, whether it's positive or negative, is much bigger than it of the riser when the friction = 0.1.

Conclusions

1. In this study, the parametric modeling technology is adopted to set up the finite element model of unbonded flexible riser composed of 10 layers. The mechanical behavior of the riser under torsion is studied with ABAQUS considered the material nonlinearity, contact interaction and friction.

2. The detailed stress and deformation results of each layer of the riser under torsional load are obtained through finite element analysis. From the results, it can be obtained that the main bearing layer in flexible riser under torsion is the tension armor (consisted of steel strips) whose strips rotate in the same direction with the torsion direction.

3. The numerical simulation computation was carried out for the flexible riser in different contact conditions. The influence on stress and deformation distribution of nonlinear boundary conditions caused by the frictional contact was studied in this study. It

concluded that the numerical simulation computation considered no friction in the riser led to larger error in the stress and deformation calculation results and also illustrated that the simplification of the friction condition in the analytical analysis can cause inaccurate calculation results.

1. J. J. Féret and C. L. Bournazel, "Calculation of stresses and slip in structural layers of unbonded flexible pipes," *J. Offshore Mech. Arct. Eng.*, **109**, No. 3, 263–269 (1987).
2. A. M. Harte and J. F. McNamara, "Modeling procedures for the stress analysis of flexible pipe cross sections," *J. Offshore Mech. Arct. Eng.*, **115**, No. 1, 46–51 (1993).
3. J. A. Witz and Z. Tan, "On the axial-torsional structural behaviour of flexible pipes, umbilicals and marine cables," *Mar. Struct.*, **5**, Nos. 2-3, 205–227 (1992).
4. D. B. McIver, "A method of modelling the detailed component and overall structural behaviour of flexible pipe sections," *Eng. Struct.*, **17**, No. 4, 254–266 (1992).
5. M. Brack, L. M. B. Troina, and J. R. M. De Sousa, "Flexible riser resistance against combined axial compression, bending, and torsion in ultra-deep water depths," in: Proc. of the Int. Conf. on Offshore Mechanics and Arctic Engineering (June 12–17, 2005, Halkidiki, Greece), Vol. 1, Paper No. OMAE2005-67404, ASME (2005), pp. 821–829.
6. J. Lanteigne, "Theoretical estimation of the response of helically armored cables to tension, torsion, and bending," *J. Appl. Mech.*, **52**, No. 2, 423–432 (1985).
7. J. F. McNamara and A. M. Harte, "Three-dimensional analytical simulation of flexible pipe wall structure," *J. Offshore Mech. Arct. Eng.*, **114**, No. 2, 69–75 (1992).
8. G. Alfano, A. Bahtui, and H. Bahai, "Numerical derivation of constitutive models for unbonded flexible riser," *Int. J. Mech. Sci.*, **51**, No. 4, 295–304 (2009).
9. A. Bahtui, H. Bahai, and G. Alfano, "A finite element analysis for unbonded flexible riser under torsion," *J. Offshore Mech. Arct. Eng.*, **130**, No. 4, 169–173 (2008).
10. J. Y. Li, Z. X. Qiu, and J. S. Ju, "Numerical modeling and mechanical analysis of flexible riser," *Math. Probl. Eng.*, **2015**, Article ID 894161, 1–7 (2015).

Received 30. 08. 2016